Article

Not peer-reviewed version

NEMUCO: The In Vitro 4D NMJ as an Innovative Powerful Tool to Study Nerve and Muscle Cell-Cell Communication

Katharina Block , Gaia Ziraldo , Gabor Trautmann , Sandra Furlan , Abhishek Singh , Sabine Grosser , Martina Gutsmann , Paola Lorenzon , Pompeo Volpe , Imre Vida , Dieter Blottner , Michele Salanova *

Posted Date: 9 March 2026

doi: 10.20944/preprints202603.0617.v1

Keywords: muscle and nerve cell co-culture; muscle synaptogenesis in vitro; neuromuscular junction development

 doi:10.20944/preprints202603.0617.v1

Article

NEMUCO: The In Vitro 4D NMJ as an Innovative Powerful Tool to Study Nerve and Muscle Cell-Cell Communication

Katharina Block [1], Gaia Ziraldo [1], Gabor Trautmann [1], Sandra Furlan [2], Abhishek Singh [1], Sabine Grosser [1], Martina Gutsmann [1], Paola Lorenzon [3], Pompeo Volpe [4], Imre Vida [1], Dieter Blottner [1] and Michele Salanova [1,*]

[1] Charité–Universitätsmedizin Berlin, Institute of Integrative Neuroanatomy, Berlin, Berlin, Germany
[2] CNR-Neuroscience Institute, Section of Padova, Padova, Italy
[3] University of Trieste, Department of Life Sciences, Trieste, Italy
[4] University of Padova, Department of Biomedical Sciences, Padova, Italy
* Correspondence: michele.salanova@charite.de; Tel.: +49-30-450528-354, Fax: +49-30-450528-954/-922; https://orcid.org/0000-0002-7066-3876

Abstract

Chronic muscle unloading, following denervation, aging, long-term bedrest as either spaceflight analog or actual spaceflight missions, results in a decline of neuromuscular junction (NMJ) structure and function, resulting in muscle mass decline and impaired fine motor control. Similar changes are also observed in several neuromuscular diseases and myopathies with signs and symptoms related to impaired movement control. Here, we report on a powerful 3D co-culture experimental model developing NMJ-like structures, as a novel *in vitro* platform for functional/regulatory studies during time (4D co-culture) for basic and translational research purpose. Murine NErve (NSC-34 motor neuron) and MUscle (C_2C_{12} myoblast) cell CO-cultures (NEMUCO) were grown on either synthetic or biological three-dimensional (3D) scaffolds. The co-cultures were analyzed using a significant array of molecular and cellular biology tools, based on NMJ-specific molecular marker expression combined with muscle- and nerve-cells specific differentiation biomarkers. Specialized cell-cell contacts were present starting at day 2 of co-culture. Triple immunostaining indicated neurofilament-positive axonal nerve terminals approaching clustered α-bungarotoxin-positive nicotinic acetylcholine receptors (nAChRs) in desmin-positive developing myotubes, representing the first signs of NMJ-like structure assembly *in vitro*. 3D reconstruction morphometry revealed a 50-nm-wide distance similar to the *in vivo* native synaptic cleft dimension. It is noteworthy that co-cultured motor neurons showed a trend of increase of SNAP-25 transcription, one of the most important SNARE proteins, whereas co-cultured myotubes showed a slight increase of junctophilin and ryanodine receptor type 1 transcription, both critical proteins of the triadic junction of differentiated muscle fibers. In most respects, neuronal-myotube cell-cell communication contacts in our 3D co-cultures mimicked native NMJ microdomains. Neuronal-myotube co-cultures grown in 3D scaffolds represent a powerful tool for investigating the molecular mechanisms underlying NMJ adaptation and plasticity in muscle myopathies. Moreover, this approach could be adapted for customized miniaturized platforms designed for cellular neurobiology research during spaceflight conditions.

Keywords: muscle and nerve cell co-culture; muscle synaptogenesis in vitro; neuromuscular junction development

1. Introduction

Chronic muscle unloading in healthy subjects and in several muscle pathological conditions, such as auto-immune neuromuscular diseases, myopathies, neuro- and poly-neuropathy,

 doi:10.20944/preprints202603.0617.v1

denervation, aging, and/or chronic muscle unloading during long-term bedrest or spaceflight missions, results in a significant decline in neuromuscular junction (NMJ) structure and function, which in turn has a significant impact on muscle mass maintenance and impaired fine motor control [1–8]. Therefore, a deeper understanding of the molecular and cellular mechanisms that lead to NMJ imbalance is of paramount importance in order to establish reliable countermeasure approaches.

The NMJ is a unique specialized muscle and nerve cell-cell communication contact that translates neuronal electrical impulses into skeletal muscle mechanical responses [9,10]. The fusion of presynaptic vesicles containing the neurotransmitter acetylcholine (ACh) at the nerve terminal membrane, provides a unique and highly efficient mechanism responsible for the selective activation of postsynaptic nicotinic ACh receptors (nAChRs) on the postsynaptic skeletal muscle membrane [11], which is required for muscle contraction [9,10].

Moreover, skeletal muscle does not only contract during movement but also fulfills many other vital physiological functions such as muscle tone, tissue homeostasis and different intra- and extra-synaptic myonuclear gene expression and translational regulation as well as synaptic plasticity [12]. Therefore, the mechanisms that translate neuronal electrical stimuli into skeletal muscle transcriptional programs and mechanical responses at the NMJ are very complex and tightly regulated, requiring a high degree of coordination between different signaling pathways and their eventual cross-talk in normal muscle function.

To date, the underlying molecular mechanisms and signaling pathways that negatively impact NMJ performance in different physiological and pathophysiological conditions remain largely unexplored.

Due to the unique characteristics of the NMJ and its complexity, in addition to technical and ethical limitations, it remains difficult to study it in human muscle *in vivo*, especially when it comes to pharmacological treatment.

With the aim to further investigate such mechanisms many efforts have been made in the last decade to establish controlled experimental model to generate the NMJ *in vitro* as close as possible to the native form. In this regard, primary cell co-cultures were initially used [13]. However, given the need for standardized experimental models, the use of immortalized cell lines, for both muscle and motor neuron cells, was adopted. Only recently, however, following the development of the innovative three-dimensional (3D) co-culture methodology and the growing interest in *in vitro* cell biology, induced pluripotent stem cells such as iPSC cells have been employed [14,15]. The use of iPSC cells allows multiple cell types and tissues to be organized within complex *in vitro* systems, which are defined as organoids, ultimately making them far more complex than 3D *in vitro* systems [16].

Overall, the use of 3D co-cultures offers a more realistic model of the physiological environment. It allows for more complex interactions between different cell types and a better imitation of tissue functionality, with greater robustness and longevity of the cell culture itself. Furthermore, this provides an interesting platform for evaluating the behavior of new chemical entities in drug development, leading to improved applications in the development of drug therapies. No less important, the application of such an experimental model could be of particular interest and a useful tool to better investigate and further elucidate the molecular mechanisms underlying the cell-cell communication contacts between muscle cells and nerve cells in different experimental environmental conditions. This experimental model could represent a powerful tool to explore the spatial and temporal hierarchical assembly of the different molecular players at the pre- and post-synaptic side, their associated signaling pathways and their potential cross-talk during muscle synaptogenesis, avoiding the use of animals. Indeed, this experimental model can be successfully implemented in engineered hardware for space science research experiments in order to further investigate molecular mechanisms of disuse-induced skeletal muscle atrophy in astronauts during long duration missions. Noteworthy, highly preserved cell viability was recently observed in NEMUCO co-cultures integrated in cellBox-3 (ScienceShells) hardware for 12 days on ground (Salanova M. et al., lab communication).

 doi:10.20944/preprints202603.0617.v1

We established a novel experimental protocol for an advanced 4D co-culture system in which differentiated nerve and muscle cells were grown on 3D scaffolds and were able to interact with each other during the time (as 4th dimension) and generated NMJ-like structures *in vitro*. Furthermore, our data demonstrated that our experimental model is characterized by advanced cell maturation degree and up-regulation of the myogenic program inherent to normal muscle development. This protocol is broadly adaptable to further investigate several models of NMJ-associated pathologies, and has the potential to gain deeper insights into the still underexplored fundamental aspects of NMJ development, maturation and maintenance.

2. Results

2.1. Native NMJ of the Soleus Skeletal Muscle of Mice

Native NMJs were stained in the soleus muscle of rodents according to [1]. Several NMJs were identified and used as native reference control. Figure 1 shows a typical NMJ from the soleus muscle without myonuclear staining (Figure 1a) and with sub-synaptic and extra-synaptic myonuclear staining (Figure 1b).

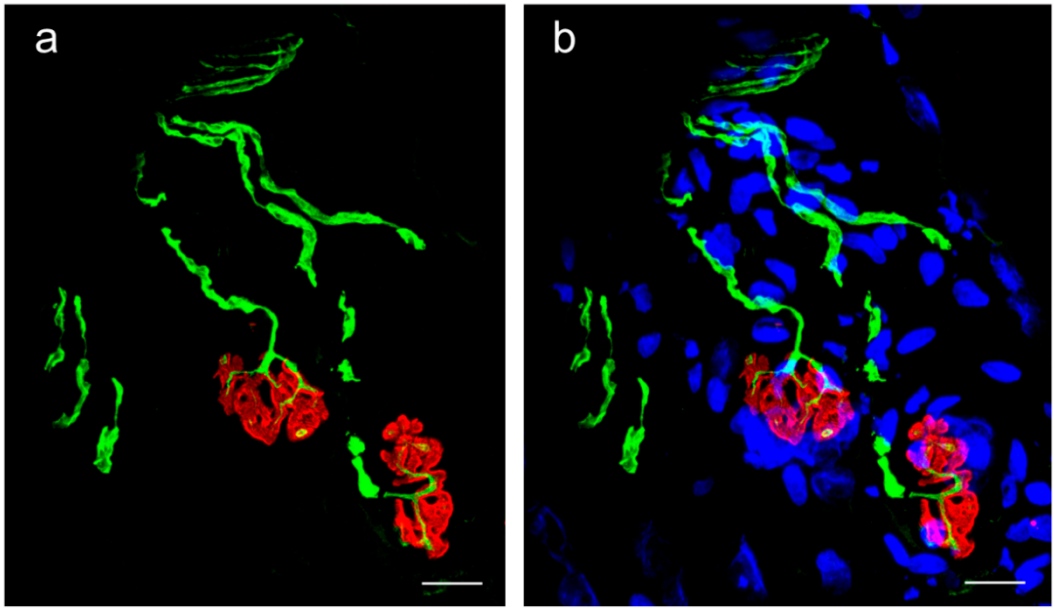

Figure 1. Laser confocal microscopy 3D-reconstruction of native NMJ of the skeletal muscle *soleus* of rat. a. Representative image of native NMJ stained with anti-neurofilaments antibodies (green) and α-bungarotoxin (red), a specific marker of nAChRs. b. Same image with counterstained nuclei / DAPI (Blue). Maximal projection of 10 stacks, 1 µm each. Magnification bar = 10 µm.

2.2. In Vitro Development of NMJs Using Non-Canonical (Synthetic) and Canonical (Biological) 3D Scaffold

To develop a reliable 3D experimental model, we established a 3D co-culture protocol for nerve and muscle cells capable of forming NMJ-like structures *in vitro*.

For this purpose, mouse C_2C_{12} myoblast cell line was used as a muscle model [17], whereas the mouse NSC-34 motor neuron cell line served as the neuronal counterpart [18].

Two different 3D scaffolds were tested: a synthetic Alvetex® polystyrene scaffold [19] and a biological scaffold consisting of highly purified extracellular matrix (ECM) hydrogel [20].

2.3. Muscle and Nerve Co-Cultures on Synthetic/Alvetex 3D Scaffold

The Alvetex® polystyrene scaffold consists of a highly porous cross-linked polystyrene material that is 200 µm thick and contains communicating voids with an average diameter of 42 µm (see in

 doi:10.20944/preprints202603.0617.v1

Figure 2). The material is designed for three-dimensional culture of mammalian cells within the scaffold. At optimal cell density, cells coexist in the same micro-niche of this highly networked material, increasing the likelihood of cell interactions and, in the case of muscle and nerve cell co-cultures, facilitating the development of specialized cell-cell contacts such as NMJs.

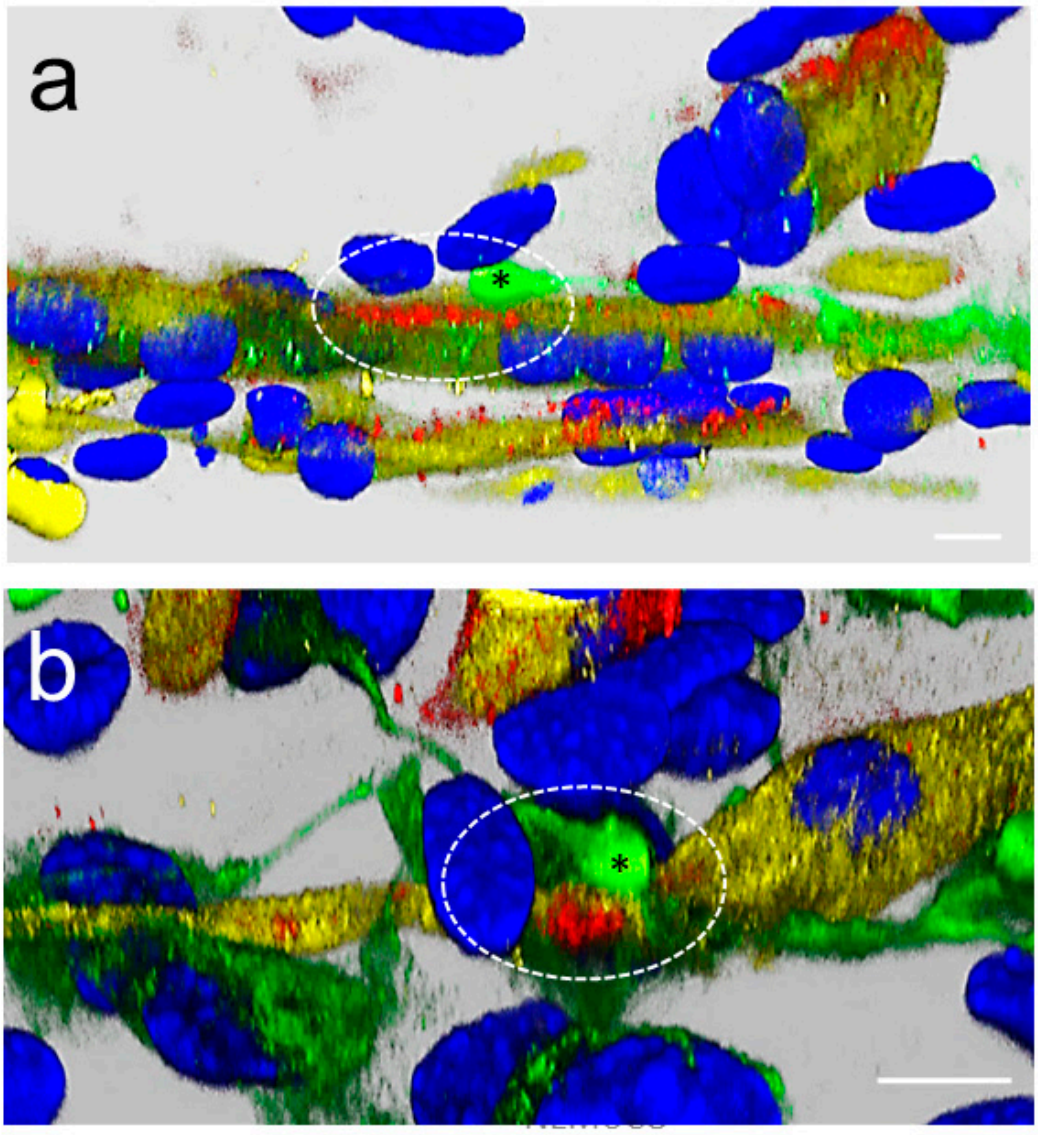

Figure 2. Laser confocal microscopy 3D-reconstruction of nerve and muscle cells 3D co-cultured on synthetic Alvetex polystyrene scaffold. (a) Representative image from early/progressive, day 2; and (b) late, day 5, stage of 3D co-cultures immunolabelled for neurofilaments (green), desmin (yellow), nAChRs (red) and nuclei (blue). White dashed oval circles: area of nerve and muscle cell-cell contact or neuromuscular junction-like structure in development. Note that the nerve endings (asterisks) approach the muscle cells at the level of prepatterned nAChR clusters. Magnification bar = 12 μm.

Myoblasts and neuronal cells were seeded on scaffolds precoated with laminin and collagen I, cultured for up to 12-14 days in medium containing nutrients and muscle- and nerve-specific growth factors (for details see Methods), and processed for immunocytochemistry at 3, 7, and 12 days of culture. Figure 2 shows a 3D reconstruction of a typical immunocytochemical image. Desmin was used as an early muscle differentiation marker; this protein forms a subsarcolemmal network across the myotube. Neurofilament proteins were used to label motor neuron axons, and α-bungarotoxin (α-BTX) was used to label nAChRs.

 doi:10.20944/preprints202603.0617.v1

As shown in Figure 2a,b (dashed circles), myotubes co-cultured with motor neurons on the 3D synthetic scaffold developed cell-cell communication contacts. Axons stained with anti-neurofilament antibodies terminated above the myotube plasma membrane near prepatterned nAChRs, suggesting developing communication contacts between myotubes and neuronal cells.

Fluorescence staining with α-BTX revealed progressive, time-dependent aggregation of nAChRs in the myotube plasma membrane, particularly near cell-cell contacts and nerve endings, suggesting the formation of NMJ-like structures in our 3D co-cultures. Progressive nAChR clustering was evident between days 2 and 5 of co-culture (Figure 2a,b, dashed circles).

By means of 3D morphological reconstruction analysis, we observed only a few myonuclei in each myotube, suggesting limited myoblast fusion during early myotube development on the 3D synthetic scaffold, possibly due to spatial constraints within the highly porous polystyrene network.

The 3D co-culture system on polystyrene synthetic scaffold very likely produced NMJ-like structures in a proper, regular, developing manner showing muscle specific differentiation markers such as contractile filaments.

However, the opaque nature of the polystyrene scaffold and the deep positioning of cells concealed within its porous structure precluded real-time phase contrast and differential interference contrast (DIC) microscopy for proper visualization.

2.4. Nerve and Muscle Cell Co-Cultures on Biological 3D Scaffolds

To circumvent the problems of low myonuclear number and reduced myotube size, we encapsulated muscle and nerve cells in extracellular matrix hydrogels, including Matrigel and collagen I. The advantages of using such hydrogels include (i) ease of processing, (ii) low cost, and (iii) flexibility in live cell manipulation. In addition, pore size, ligand density, and hydrogel stiffness can be adjusted by modifying the concentration of matrix components, thereby facilitating modification of the hydrogel's microstructural properties. Thus, the hydrogel supports cell differentiation by providing an environment that mimics the native extracellular matrix (ECM) *in vivo*. Motoneurons were seeded on top of the hydrogel containing differentiated myotubes, creating spatially distinct microenvironments, however supporting cell-cell interactions and subcellular compartments.

Three different hydrogel concentrations were initially tested to identify the optimal formulation supporting myoblast differentiation and fusion, as well as motor neuron differentiation and axonal sprouting. The optimal formulation consisted of 30% collagen I and 20% Matrigel, which provided ideal conditions for both muscle and nerve cell differentiation.

Figure 3a-f show different developmental stages of the 3D muscle and nerve cell co-culture as visualized by differential interference contrast (DIC) microscopy. Figure 3a shows proliferating myoblasts at culture day 1. Figure 3b shows elongated myoblasts fusing into myotubes. Figure 3c shows maturing myotubes with a typical cross-striated pattern, indicating increased assembly of the contractile apparatus. Figures 3d-f show individual motor neurons (arrows) contacting maturing myotubes.

Notably, myotubes cultured in the hydrogel scaffold contained 10-20 times more myonuclei than those on the polystyrene scaffold, indicating enhanced myoblast fusion. Co-cultures were maintained for 1-2 weeks to allow complete differentiation.

Figure 4 shows a bright field image from a live cell video of the co-culture. Arrows indicate a motor neuron axon extending toward a myotube. The arrowhead (inset TOP right) marks the nerve terminal in contact with the myotube (dashed box in overview), suggesting a developing NMJ-like structure. The inset shows a magnified view of the contact site (arrowhead).

 doi:10.20944/preprints202603.0617.v1

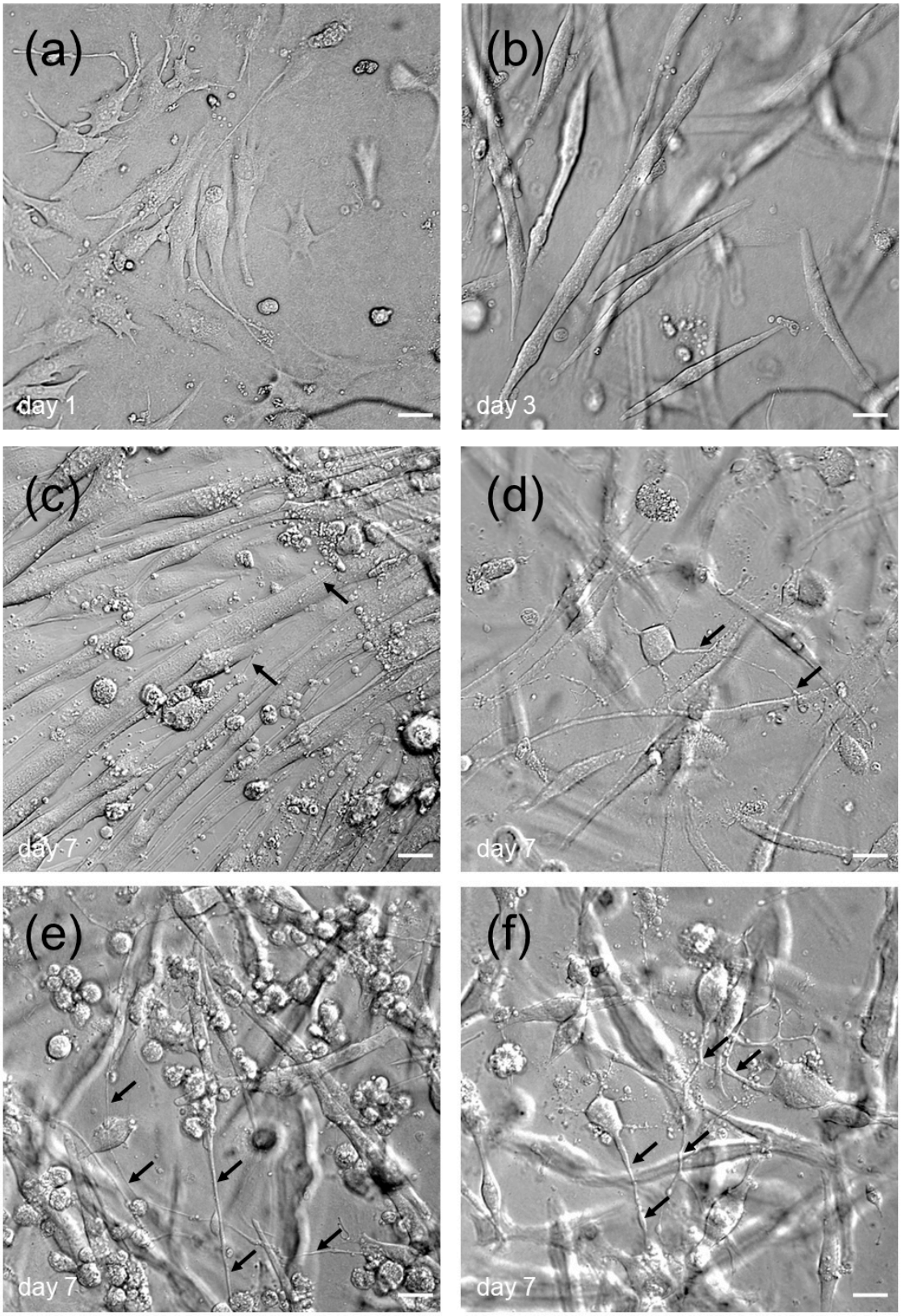

Figure 3. Differential interference contrast (DIC) microscopy of differentiating mouse C_2C_{12} myoblasts and NSC-34 α-motoneurons 3D co-cultures. (a) Proliferating myoblasts, 1-day *in vitro* culture. (b) Differentiating fusing myoblasts, 3-days in culture. (c) Maturing myotubes with a typical cross-striated pattern and α-motoneuron with a prominent axon (arrows) are clearly visible, 7-days in co-culture. (d) α-Motoneuron (top) with a prominent axon (arrows) and with myotubes (bottom) is visible, 7-days in co-culture. (e, f) Co-cultures with several myotubes and α-motoneurons with prominent axon (arrows) at different z-axis levels. Magnification bar: 25 μm.

 doi:10.20944/preprints202603.0617.v1

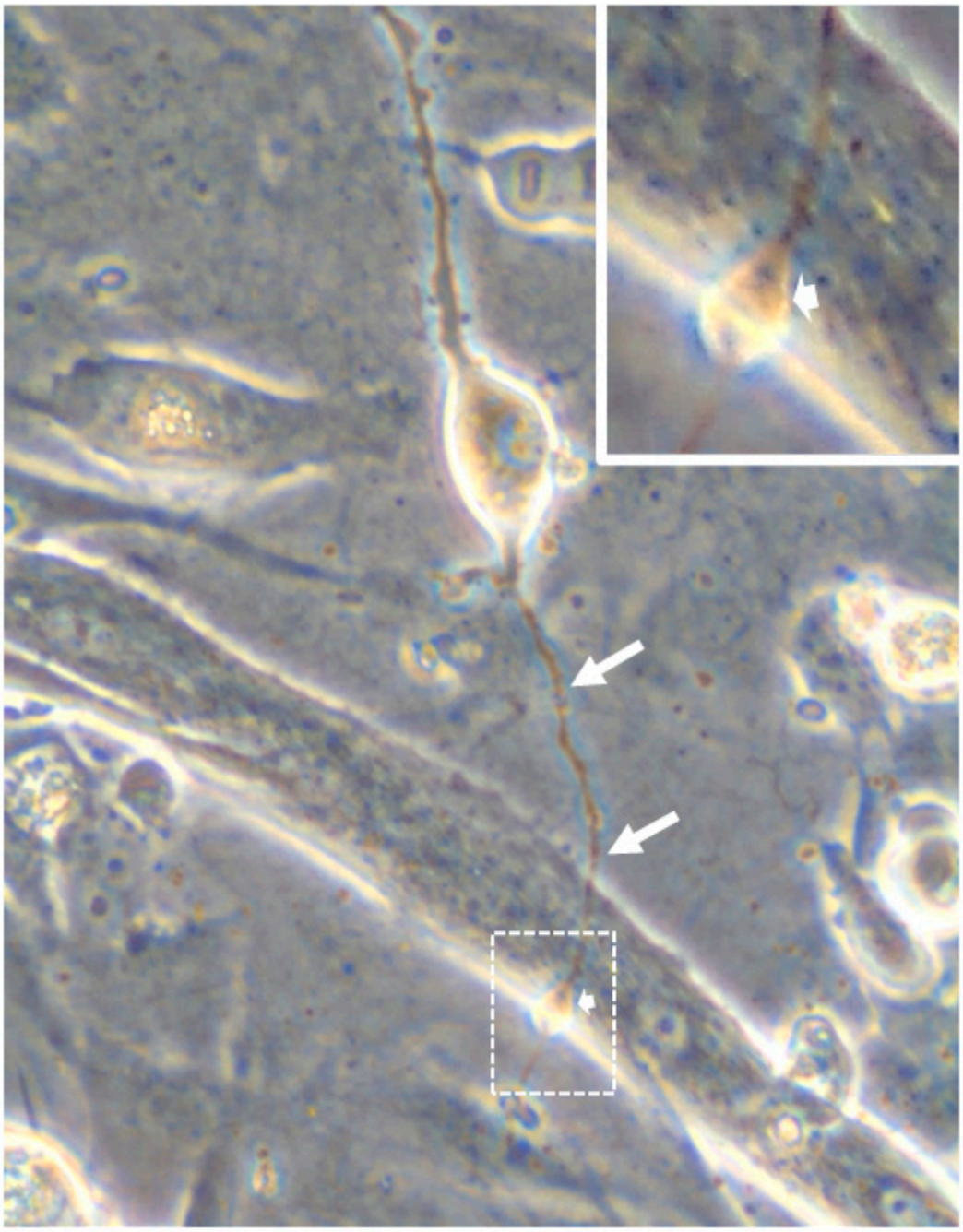

Figure 4. Bright field image of mouse C_2C_{12} muscle myotubes and NSC-34 α-motoneuron 3D co-culture on hydrogel scaffold. A well-differentiated α-motoneuron with a relatively long axon (arrows) is present in contact with a small myotube and, more likely, the large myotube located at a lower level (5-days of co-culture). White dashed box: developing specialized muscle and nerve cell-cell contact (arrowhead) close to the nerve ending. Inset: Magnification of the dashed box showing the nerve ending (arrowhead) in contact with the myotube and a branched axon extending above a differentiated myotube. Representative frame was extracted from a live cell video imaging acquired with a Leica microscope (Obj. 40x) using the HD camera MC170.

To assess muscle cell maturation and NMJ formation in the hydrogel scaffold, we performed immunocytochemistry using cell-type-specific differentiation markers and NMJ-specific markers.

Figures 5 and 6 show the expression pattern of fast-type myosin heavy chain ($_f$MyHC) in co-cultured myotubes. Notably, by $_f$MyHC immunohistochemistry experiments revealed that myotubes contacted by α-motor neurons exhibited improved organization of the cytoskeleton and contractile

 doi:10.20944/preprints202603.0617.v1

apparatus, forming cross-striated patterns characteristic of sarcomere-like structures in adult skeletal muscle, (Figures 5 and 6).

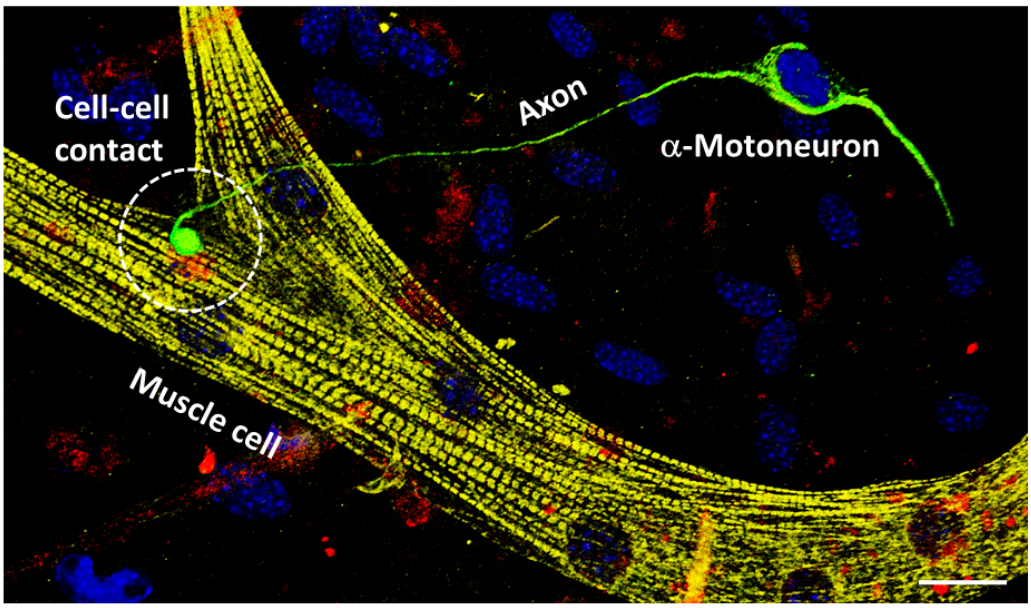

Figure 5. Laser confocal microscopy of nerve and muscle 3D co-culture. Triple-staining experiment in maturing myotubes and α-motoneuron with anti-fMyHC (yellow), anti-neurofilament (green) antibodies, and nAChRs (red) (7-days in co-culture). Nuclei/DNA were counterstained with DAPI (blue). White dashed ring: axon terminal ending contact on pre-patterned postsynaptic nAChRs suggesting the presence of developing NMJ-like structures in the co-culture. (Maximal projection of 10 stacks, 1 µm each). Magnification bar = 15 µm.

To further study NMJ development, structure, function, and stability under microgravity conditions, cells were grown in the CellBox-3 (ScienceShells) hardware, i.e. a closed, automated cell culture system. This served as a pilot experiment for the planned NEMUCO spaceflight mission aboard the International Space Station (ISS).

Figure 6 shows that NEMUCO co-cultures thrived in the perfused microchambers, expressing appropriate nerve- and muscle-specific differentiation markers, such as axonal neurofilaments and fMyHC-positive contractile filaments. Notably, the co-cultures formed cell-cell contacts within the CellBox-3 hardware, validating the system's suitability for spaceflight experiments.

Digital interference contrast (DIC) microscopy provides a reliable, high-resolution tool to investigate 3D-structures of three-dimensional cell co-cultures and, in particular, unambiguous visualization of specialized cell-cell contacts. DIC microscopic imaging was performed with the 3D cocultures grown in hydrogel. Figure 7 shows a representative DIC image of the co-cultured muscle and nerve cells, revealing a motor unit-like networking structure *in vitro* (dashed rings). As shown in Figure 7, a large α-motoneuron positioned above the myotubes with its long-branched axon and nerve terminals, contacts several myotubes located at different focal planes (dashed circles) suggestive of typical NMJ-like structures and thus recapitulating the classic feature of a motor unit.

Taken together, these results demonstrate that co-cultures of nerve and muscle cell lines grown on biological hydrogel 3D scaffolds develop specialized nerve-muscle cell-cell contacts, such as NMJs, as evidenced by the expression of nerve-, muscle-, and NMJ-specific molecular markers.

 doi:10.20944/preprints202603.0617.v1

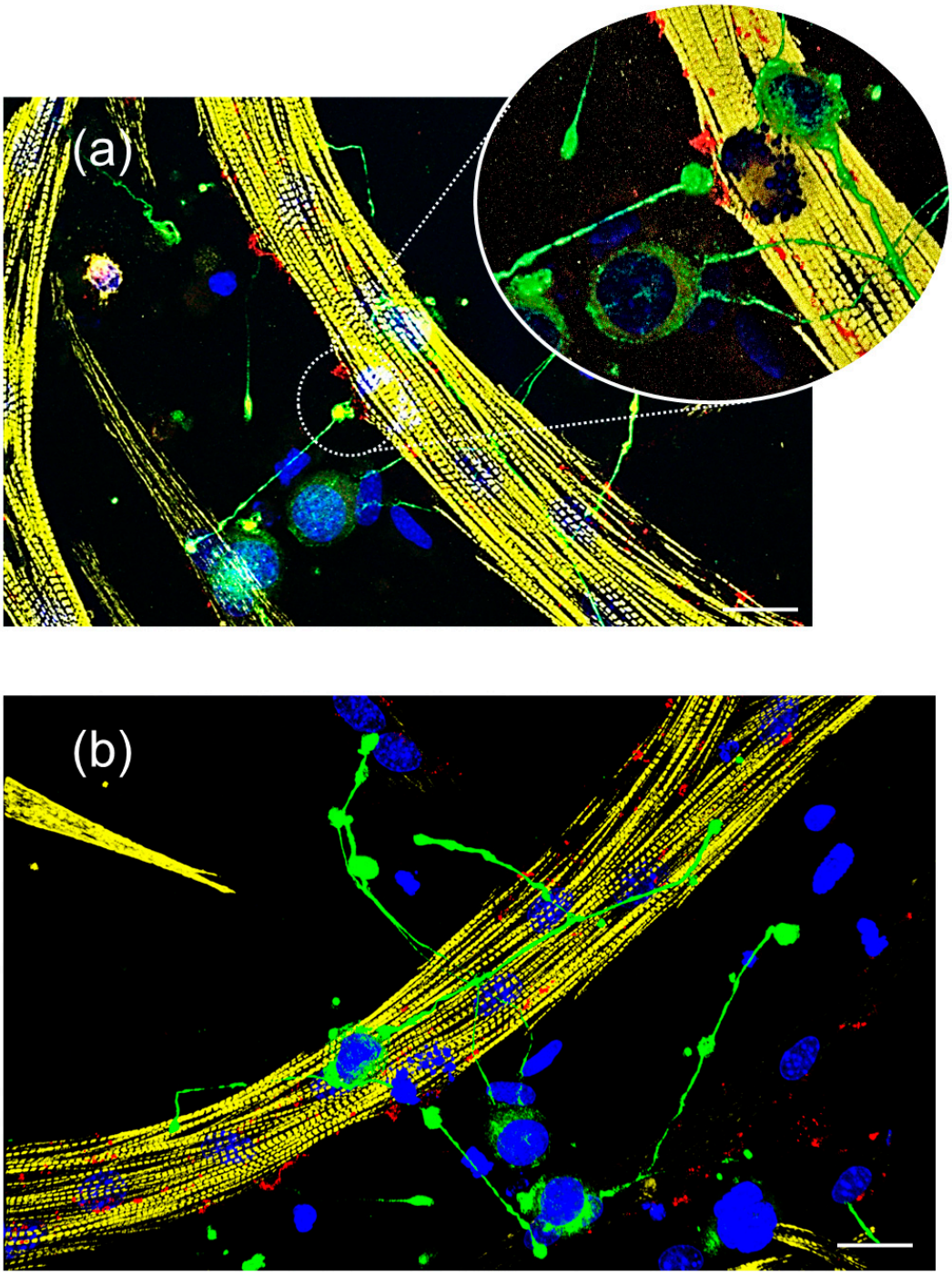

Figure 6. Laser confocal microscopy 3D-reconstruction of muscle and nerve cell co-cultures in a hydrogel scaffold within the CellBox hardware. (a) Maturing myotubes (yellow) stained with monoclonal anti-fMyHC antibodies; α-motorneurons (green) stained with monoclonal anti-neurofilaments antibodies; prepatterned nAChRs (red) stained with α-BTX; nuclei/DNA (blue) were counterstained with DAPI. Insert is a magnification of nerve and muscle cell-cell contact. Magnification bar = 15 μm. (b) Co-culture immunostaining as in (a), shows another area of the same field with higher nerve cells density and long axons (green). Magnification bar = 15 μm.

 doi:10.20944/preprints202603.0617.v1

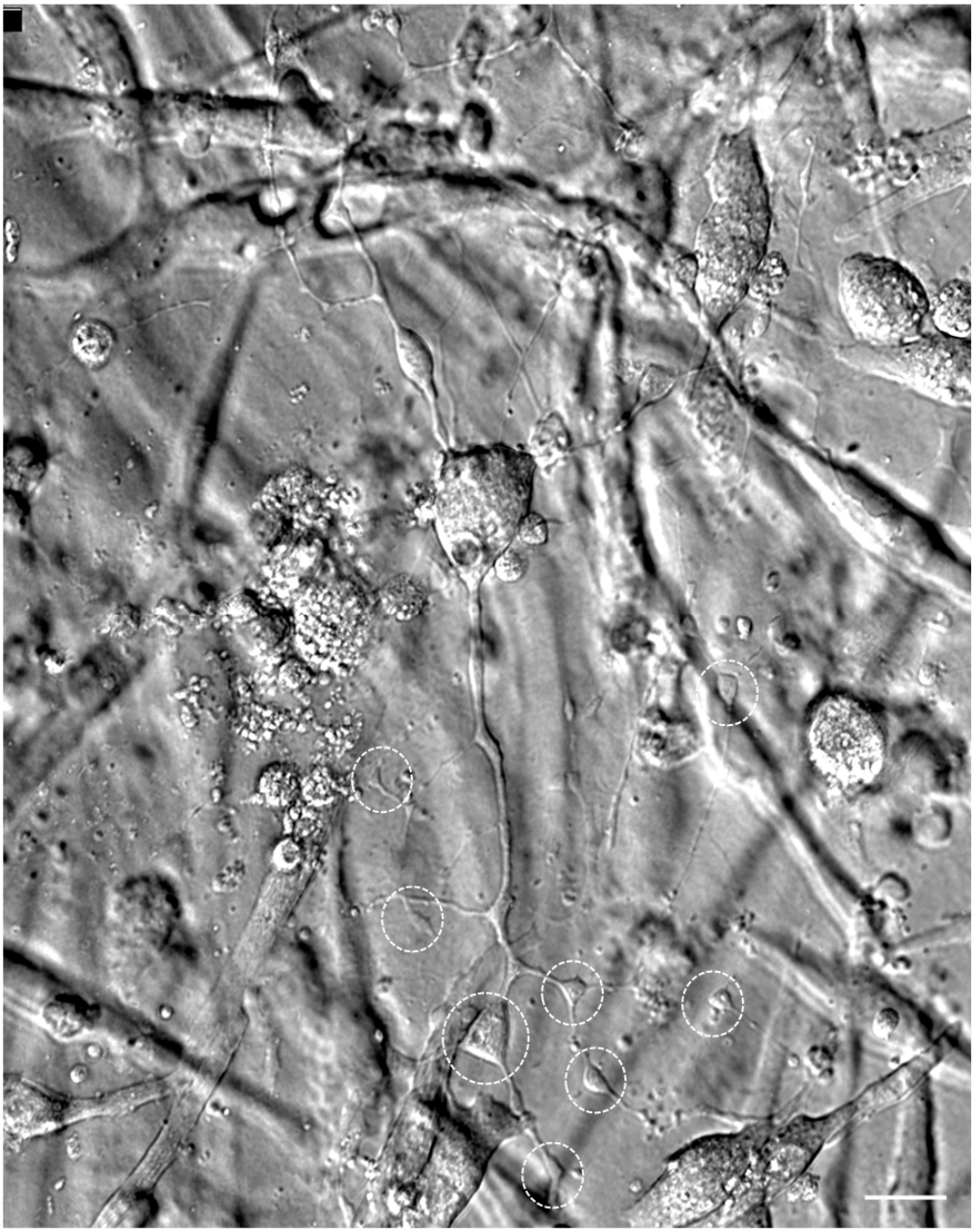

Figure 7. Differential interference contrast (DIC) microscopy of motor-unit-like network structures formed by differentiating mouse C_2C_{12} myoblasts and NSC-34 α-motoneurons in 3D co-culture on a hydrogel scaffold. Nerve motoneuron and muscle myotube cell in focus. α-Motoneuron at the top, with a prominent branched axon and terminal nerve terminals (dashed circle), and several myotubes at the bottom are visible (7-days in co-culture). Magnification bar = 25 μm.

2.5. Nerve-Independent nAChRs Prepatterning on Biomatrix 3D Scaffolds

Figure 8 shows the prepatterning of AChRs in aneural muscle myotube plasma membranes, as revealed by α-BTX staining (red label), presumably due to neural agrin present in the culture medium. This suggests nerve-contact independent nAChRs prepatterning in our 3D experimental model.

 doi:10.20944/preprints202603.0617.v1

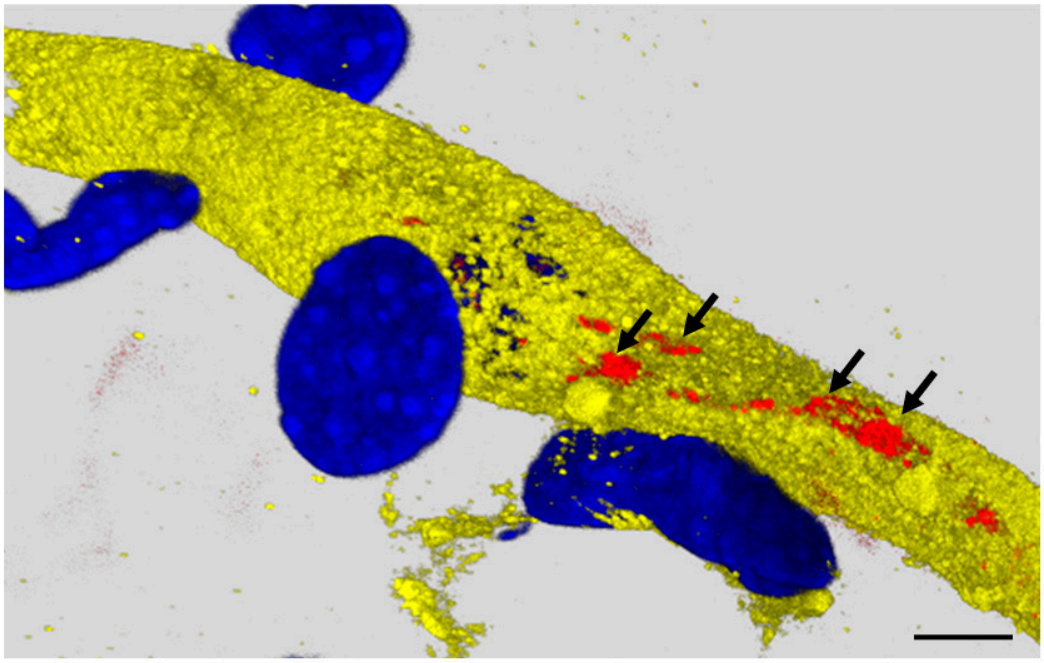

Figure 8. Laser confocal microscopy 3D reconstruction of prepatterned nAChRs in aneural cultured myotubes. Maturing myotubes were triple stained with anti-desmin antibody (yellow), Alexa555-conjugated α-BTX (red) and DAPI (blue). Areas of increased concentration, or pre-patterning of nAChRs (arrows), are inferred by α-BTX staining. Magnification bar = 15 μm.

2.6. Synaptic Cleft 3D Reconstruction and Morphometric Analysis

Figure 9 illustrates the results of morphometric analysis performed on representative NMJs developed on polystyrene synthetic scaffolds (upper panel) and hydrogel biological scaffolds (lower panel) using customized LAX software (Leica Microsystems). Images were first processed, and the resulting binary images were used as input for measuring the distance between axon terminals and acetylcholine receptor regions. We measured the area where the intensity of Population 1 (axon/neurofilament, NF) decreases and the intensity of Population 2 (AChR) increases, which provides quantitative information about the distance between these two regions. Interestingly, the distance of the first measured NMJ-like area (polystyrene synthetic scaffold) is approximately 88 nm, whereas the distance of the second measured NMJ-like area (hydrogel biological scaffold) is approximately 50 nm. These results are comparable to the size of the synaptic cleft in skeletal muscle *in vivo*.

Taken together, morphometric analysis revealed that specialized cell-cell contacts and NMJ-like structures formed in our 3D co-culture system exhibit synaptic cleft dimensions comparable to those of native NMJs in skeletal muscle *in vivo*, thereby validating the reliability and physiological relevance of our 3D co-culture experimental model.

 doi:10.20944/preprints202603.0617.v1

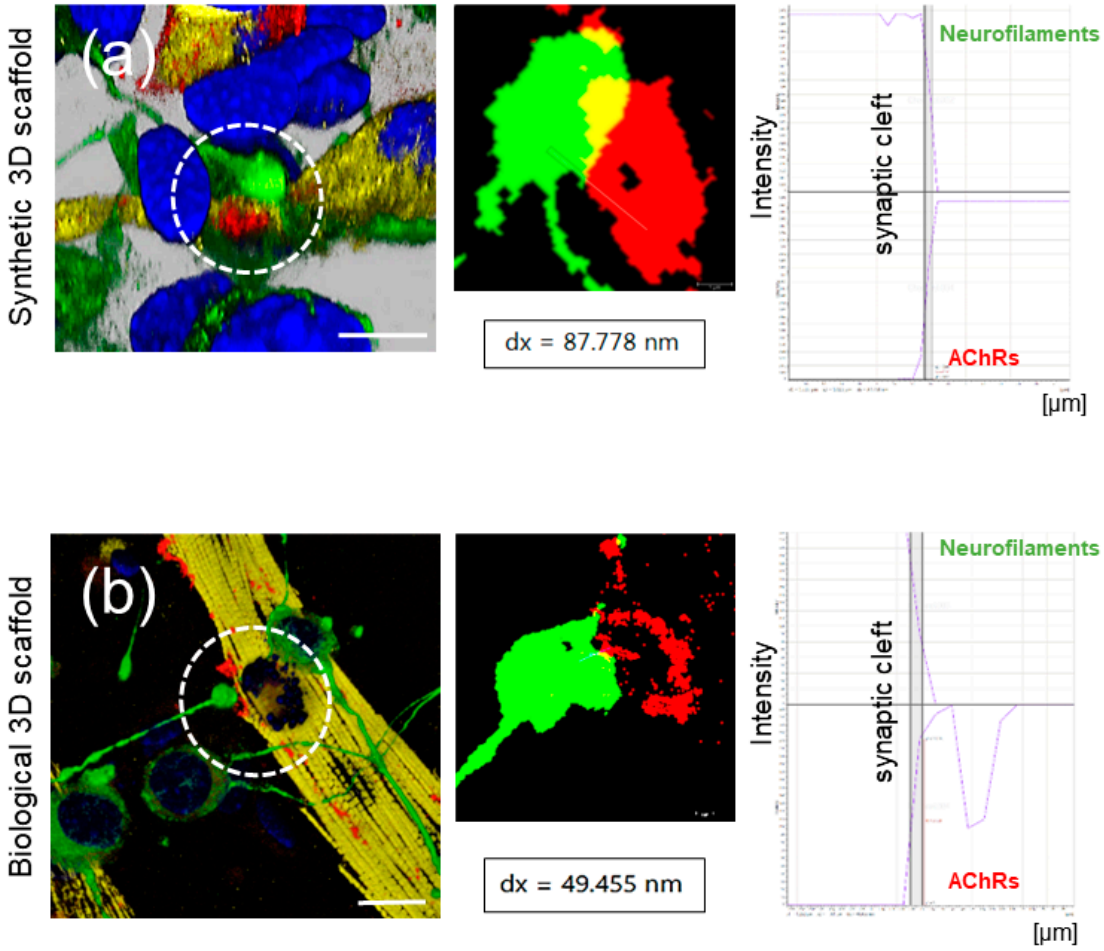

Figure 9. Morphometric analysis of synaptic cleft distance by laser confocal microscopy. (a) Left panel: maturing muscle and nerve cells in 3D co-culture on Alvetex scaffolds; middle panel: quantification of synaptic cleft distance. Magnification bar = 12 µm. (b) Left panel: maturing muscle and nerve cells in 3D co-culture on hydrogel scaffolds; middle panel: quantification of synaptic cleft distance. White dashed circles highlight regions of neuromuscular contacts indicating developing NMJ-like structures. Magnification bar = 15 µm. dx= distance.

2.7. Western Blot Analysis

Total protein extracts from both myotubes monocultures and co-cultures in hydrogel were investigated for the expression pattern of the structural protein desmin, a well characterized early marker of skeletal muscle development, which plays a key role on the stability of muscle sarcomere and membrane architecture.

Desmin content was investigated by Western blot using a specific monoclonal anti-desmin antibody. As shown in Figure 10a, a desmin immunoreactive band consistent with the desmin predicted MW of 53 kDa (Figure 10a: upper band, arrow), was present in all monocultured and co-cultured myotubes. However, densitometric analysis revealed no significant differences between monocultures and co-cultures (Figure 10b, left panel). An additional, low intensity desmin immunoreactive band of approx. 50 kDa, referable to the immature form of desmin, was present in all monocultured and co-cultured myotube samples (Figure 10a: lower band, arrowhead). Notably, densitometry showed a trend of increase of the immature form of desmin (Figure 10b: right panel) in either co-cultured myotubes or myotubes grown in the presence of α-motoneuron nerve cells compared to myotube monocultures (Figure 10a, b). These results are consistent with the increased myogenic activity in 3D co-cultured myotubes compared to myotube monocultures.

 doi:10.20944/preprints202603.0617.v1

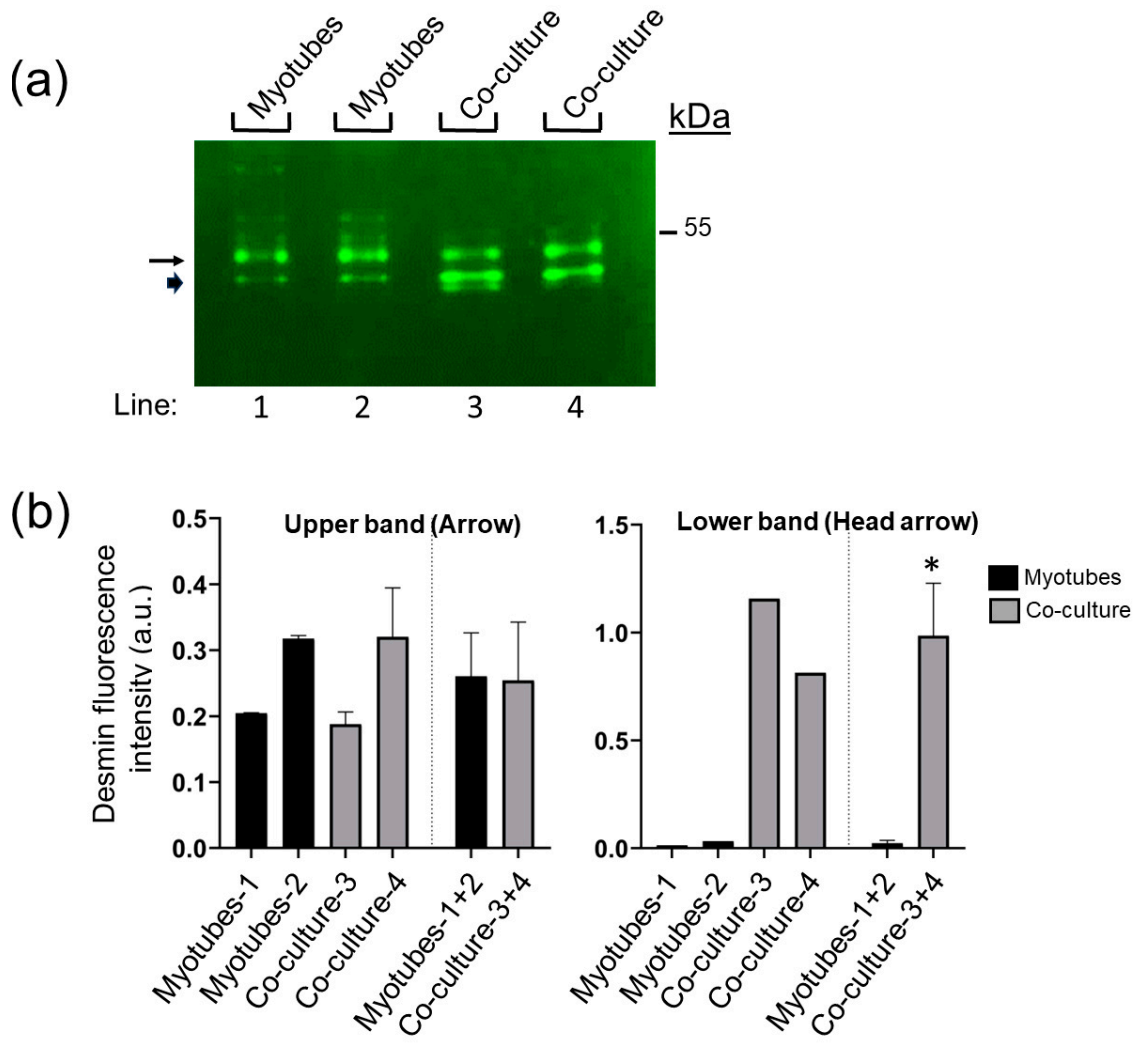

Figure 10. Desmin Western blot analysis of monocultured myotubes (Myotubes) and co-cultured myotubes with *α*-motoneuron nerve cells (Co-culture). a. Representative Western blots with two replicates of cell extracts from monocultured myotubes (lanes 1 and 2) and co-cultured nerve-myotubes (lanes 3 and 4). Both, the mature form of desmin (upper band, arrow) and the immature one (lower band, arrowhead), are present. b. Left panel, densitometric analysis of the 53 kDa desmin content. b. Right panel, densitometric analysis of the 50 kDa desmin content.

2.8. Quantitative qPCR Gene Expression Analysis

Levels of jph-1, RyR1 and SNAP-25 mRNA transcripts were measured in total mRNA extracts from muscle and nerve cell monocultures and co-cultures at *in vitro* days 0, 4, 7, 11, 14, and 18 for monocultures and days 1, 4, 8, 11, and 15 for co-cultures. The results clearly showed that in the presence of NSC34 motoneurons, myotubes exhibited a slight increase in transcription of both jph-1, a structural proteint connecting the plasma membrane to the sarcoplasmic reticulum terminal cisternae (important component of the triadic junction), and RyR1, the major intracellular calcium release channel regulating muscle contraction. The developmental expression of both proteins *in vitro* reflects the increased organization and maturation of the triadic junction and excitation-contraction coupling machinery (Figure 11 a-d).

 doi:10.20944/preprints202603.0617.v1

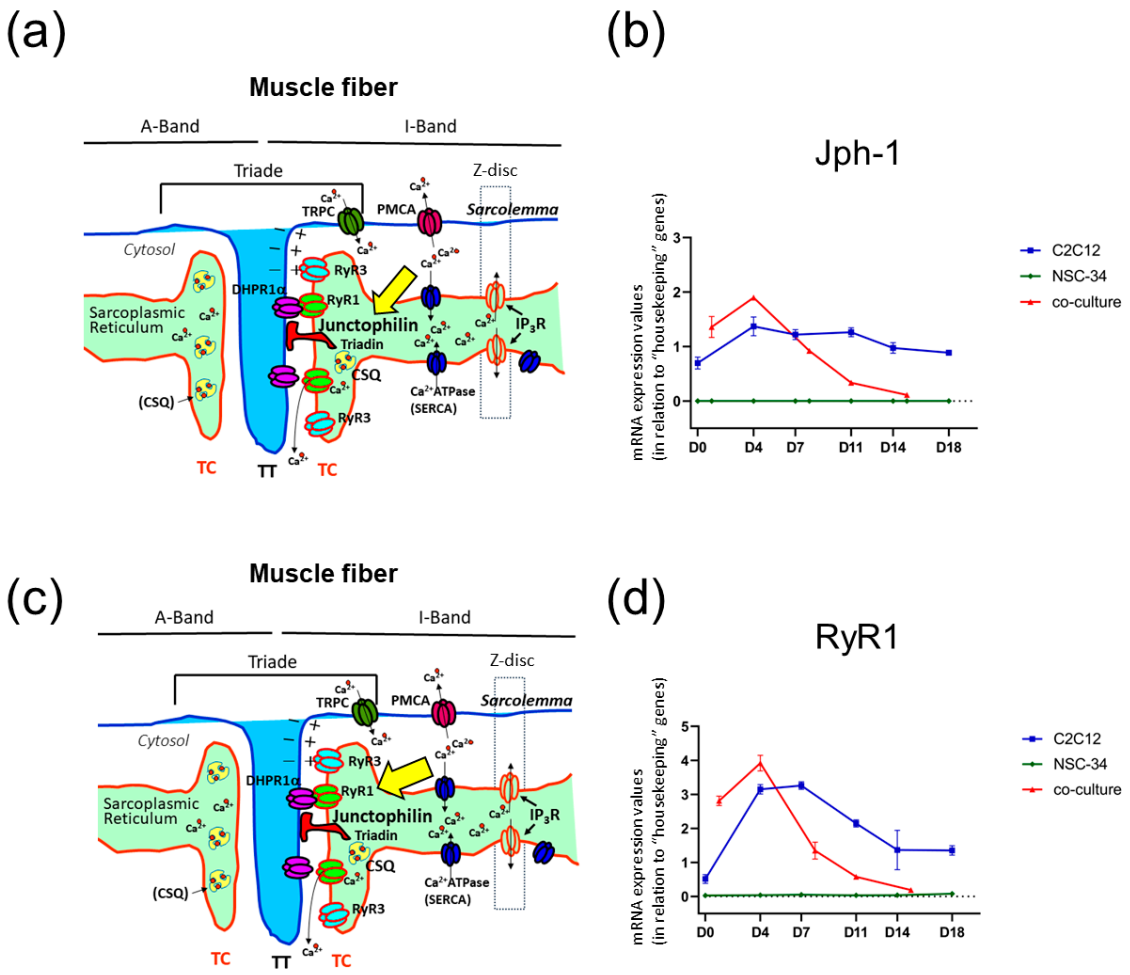

Figure 11. qPCR transcription analysis of RyR1, jph-1, and SNAP-25. (a) Diagram representing molecular players including Jph-1(yellow arrow) at the muscle triadic junction. (b) RT-PCR analysis of the triadic junction protein jph-1 in myotubes, α-motoneurons and 3D co-cultures. (c) Diagram representing molecular players including RyR1 (yellow arrow) at the muscle triadic junction. (d) RT-PCR analysis of RyR1in myotubes, α-motoneurons and 3D co-cultures.

Similarly, elevated transcription of SNAP-25 (a SNARE family presynaptic vesicle key protein) was found in α-motoneurons and myotube co-cultures (Figure 12 a-c). Figure 12c shows SNAP-25 transcriptional activity in α-motoneurons from co-cultures compared to monocultures, as assessed by qPCR. Data were normalized to *in vitro* day 0 control groups (myotubes and NSC-34 neurons in monoculture). As expected, SNAP-25 transcription was upregulated in co-cultures.

Thus, transcription regulation of key pre- and postsynaptic developmental proteins was consistent with NMJ maturation.

 doi:10.20944/preprints202603.0617.v1

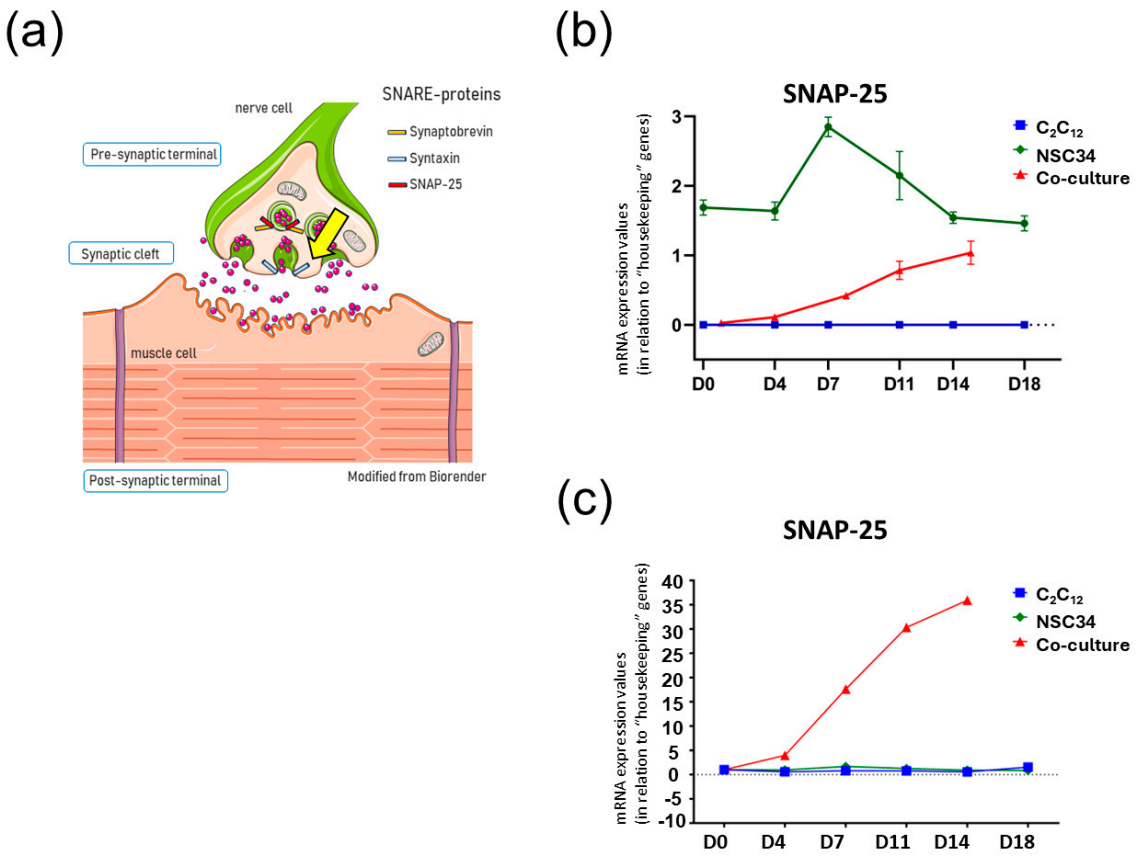

Figure 12. qPCR transcription analysis of SNAP-25. (a) Diagram representing the role of SNARE proteins at the presynaptic side (yellow arrow). (b) RT-PCR analysis of SNAP-25 in single myotubes, single α-motoneurons and 3D co-cultures. (c) RT-PCR analysis of the SNARE protein SNAP-25 in myotubes monoculture, α-motoneurons monoculture, and 3D co-cultures. Values were normalized to Day-0 control. .

3. Discussion

We report here on the comprehensive molecular and cellular characterization of an *in vitro* 3D neuronal-myotube co-culture model grown in a biological hydrogel matrix as a novel, standardized, and highly reliable tool for modeling NMJ structure, development, and functional adaptation in peripheral neuromuscular communication. The established co-culture model embedded in an optimized, highly viscous biological hydrogel, provided reliable micro-morphometric evidence (high-resolution DIC/laser confocal microscopy) as well as multiple molecular signatures of proper *in vitro* cell-cell contact assembly, including pre- and postsynaptic protein biomarkers such as SNAP-25/AChR and specific triad junction proteins Jph-1/RyR1. The 3D cell model appears to recapitulate both early events (axonal outgrowth and target cell contact) and subsequent consolidation of neuromuscular synaptogenesis under highly controlled *in vitro* conditions. This established 3D scaffold-based *in vitro* model could potentially be used for various experimental applications in research laboratories and may also serve as a feasible, resilient, and reproducible cell model for microgravity research in spaceflight.

Morphometric and cellular characterization in 3D-cultures. Clusters or prepatterned nAChRs progressively increased on myotubes plasma membrane and were subsequently approached by nerve terminals supporting the myocentric model [21–23] as documented by morphological, cytochemical and immunocytochemical analyses.

Moreover, live cell imaging showed an apparent increased myotube contractility in co-cultures above the spontaneous threshold. However, an accurate quantification was not performed because this is an issue that will be addressed in a subsequent study. Furthermore, innervated C_2C_{12} myotubes

 doi:10.20944/preprints202603.0617.v1

were characterized by the increase expression of both desmin and fast-type myosin heavy chain protein (both differentiation markers). In addition, morphological analysis revealed *in vitro* differentiation of skeletal myotubes displaying the typical cross-striated pattern or sarcomere-like structures, resulting from developmentally driven increase in muscle-nerve cell-cell communication. Interestingly, high resolution differential interference contrast (DIC) microscopy unequivocally showed that large α-motoneurons with elongated and branched axons (i.e., sprouting) were in close contact with several maturing myotubes nearby. Similar organizations are typically known as "motor units" in normal skeletal muscle physiology.

Because structure and function are intrinsically linked, we speculate that in our 3D co-culture experimental model, cell-cell communication contacts were most likely also functional. However, due to limitations imposed by the hydrogel matrix, electrophysiological data could not be obtained from the co-cultures. Nevertheless, evidence supporting this hypothesis comes from morphometric analysis, which showed that synaptic cleft distances (determined by high-resolution DIC and laser confocal microscopy) in both types of 3D scaffolds were very similar to those of native NMJs in skeletal muscle. Additionally, quantitative RT-PCR analysis revealed that co-cultured nerve cells exhibited a trend of increase in SNAP-25 mRNA transcription and slight increases in the triad junction-specific proteins Jph-1 and RyR1. Given that, only 10% to 20% of the cell co-culture is represented by motoneurons, and their difference in terms of cell size with respect to myotubes, then the observed changes in mRNA transcription of SNAP-25 might be representative. Moreover, given the essential role of SNAP-25 at presynaptic plasma membrane active zones, the trend of increase transcriptional activity of this protein in co-cultured nerve cells fully correlated with the morphological, morphometric, and immunocytochemical results, suggesting that our *in vitro* 3D co-culture model is able to recapitulate proper structural and molecular assembly of NMJ-like axon-myotube contacts.

2D and 3D NMJ modeling in vitro. Several studies have previously attempted to model the NMJ *in vitro* using 2D and 3D co-cultures with either primary or immortalized nerve and muscle cell lines, or alternatively, induced pluripotent stem cells (iPSC)-derivate organoid, for both functional and regulatory studies. A large body of evidence supports the reliability of 2D and 3D *in vitro* models for studying neuromuscular diseases involving NMJ injury or dysfunction, including peripheral motor neuron disorders and neurodegenerative and neuroimmunological diseases [24–29]. However, while such *in vitro* systems employ sophisticated tissue engineering tools and cell networks closely resembling *in vivo* systems, they often lack reproducibility and standardization, resulting in inconsistent data collection and interpretation. Interestingly, a parallel study using the same nerve (NSC-34) and muscle (C_2C_{12}) cell types in a transwell co-culture system and 2D migration co-culture demonstrated significant activation of myogenesis and synaptogenesis in co-cultured versus monocultured cells [30], corroborating the results reported in the present study. However, the transwell method is better characterized for studying chemotaxis in cells with invasive properties, such as tumor cells [31], rather than physical cell-cell contacts in co-culture [30]. Moreover, their morphological/histochemical data provide evidence of α-BTX-labeled AChR clusters with no co-staining of specific axonal markers. Therefore, there is no direct evidence of the presence of NMJ-like structures in their co-culture system. Moreover, according to the "myocentric" model [21,32], the authors cannot fully exclude the hypothesis that this is the result from paracrine mechanisms of aneural prepatterned AChR clusters.

Despite many previous studies successfully modeling the NMJ *in vitro* in 2D and 3D, none have demonstrated the NMJ *in vitro* with the resolution and comprehensive characterization presented here at the structural/morphological, morphometric, immunocytochemical, and molecular levels. Thus, we conclude that our experimental model represents a reliable and powerful tool for exploring *in vitro* molecular mechanisms of NMJ adaptation and plasticity under healthy culture conditions and in different pathophysiological settings, such as neurodegenerative and autoimmune diseases like myasthenia gravis [33]. Alternatively, it can be applied under increased or decreased oxidative stress conditions or altered gravity conditions such as simulated and/or real microgravity (spaceflight

 doi:10.20944/preprints202603.0617.v1

experiments aboard the International Space Station, ISS), which in some ways mimic muscle unloading in patients on Earth suffering from chronic immobilization.

3D scaffolds for in vitro NMJ research. As shown in our results, the demonstrated cell viability and development of NMJ-like structures in a closed and automated cell support system such as the CellBox hardware [34] on Earth indicate that the NEMUCO experimental model represents a powerful and reliable tool for studying NMJ development, maturation, and stability under different environmental culture conditions, including chronic exposure to microgravity. In this regard, the "NEMUCO-Biomission Spaceflight Experiment" is part of the current European Space Agency (ESA) Research Program, scheduled for launch to the ISS in spring/summer 2026.

Skeletal muscle adaptations during chronic disuse in various muscle disease conditions are sensed at the neuromuscular junction [1,2,7]. The most relevant changes include decreased numbers of synaptic vesicles and neurotransmitter content [35,36], degeneration of axonal terminals, and axonal sprouting [37]. Adult NMJ undergo continuous remodeling under normal physiological conditions. Extended periods of increased or decreased neuromuscular activity more extensively stimulate remodeling, including continuous changing of overall NMJ microstructure and size.

Morphological alterations of the NMJ in response to reduced neuromuscular activity and the role of exercise in maintaining integrity have been extensively described [36,38]. Interestingly, in all models of disuse-induced muscle atrophy (bed rest, denervation, limb immobilization), the NMJ experiences disruptive structural adaptations similar to those observed during microgravity exposure. For instance, loss of motor units following denervation and muscle unloading results in a metabolic shift from slow/oxidative toward fast/glycolytic phenotypes [37,39,40], as well as mitochondrial alterations and increased oxidative stress [41–43].

Skeletal muscle not only contracts but also maintains different mechanisms of intra- and extrasynaptic myonuclear gene expression and translational regulation, thus supporting synaptic plasticity. However, the mechanisms translating neuronal electrical stimuli into skeletal muscle transcriptional and mechanical responses in different physiological and/or pathophysiological processes are complex and require highly coordinated signaling pathways and their cross-talk.

Therefore, the molecular mechanisms and underlying factors that negatively influence NMJ performance during acute and/or chronic muscle unloading in health or neurodegenerative diseases, leading to muscle atrophy, remain largely unexplored.

Study Limitations. Due to its unique complexity and methodological limitations, studying the human NMJ at the cellular and molecular level *in vivo* is challenging, especially regarding effects of pharmacological treatments and testing. Therefore, information about fundamental aspects of NMJ structural and ultrastructural adaptations, development, maturation, and maintenance *in vivo* has primarily come from animal experimental models [35,44–48]. We conclude that the availability of a reliable nerve and muscle 3D co-culture model provides a unique and valuable experimental tool for further investigating and better understanding of the cellular and molecular mechanisms of NMJ adaptation and plasticity, thus providing a powerful alternative to the use of animal models.

4. Material and Methods

4.1. Cell culture C_2C_{12}

Murine C_2C_{12} myoblasts (ATCC, CRL-1772) were plated in T75 flasks coated with 0,2% gelatin and maintained in Growth medium (GM), Dulbecco's modified Eagle's medium containing 4.5 g/L glucose (DMEM; Gibco, Thermo Fisher Scientific, Inc., Waltham, MA, USA, 11960044)) with 10% heat inactivated fetal bovine serum (FBS; Sigma, St. Louis, MO, USA, F9665) and Penicillin-Streptomycin-Glutamine (100X) (Gibco, 10378016) at 37 °C in an atmosphere of 5% CO_2. Cells should be subcultured prior to cells reaching confluency (subculture at 60-70% confluency). Cells were detached with Trypsin/EDTA (0,5%) (Gibco, 15400054). Cell cultures are never grown beyond 90 % confluency, as this will result in their differentiation into myotubes. Cultures were used until passage 3.

 doi:10.20944/preprints202603.0617.v1

To induce differentiation, C_2C_{12} cells were grown to 80% confluence prior to media change for differentiation medium (DM) standard DMEM (Gibco, 11960044) containing B27 (50x) (Gibco, 17504001), murine IGF-1 (Peprotech, Rocky Hill, NJ, USA, 250-19), BDNF (Stem cell Technologies, Vancouver, BC, Canada, 78005), GDNF (Stemcell Technologies, 78058), retinoic acid (BioGems, Westlake Village, CA, USA, 3027949), and Penicillin-Streptomycin-Glutamine (100X) (Gibco). Cultures were replenished with fresh medium every two days.

4.2. Cell culture NSC-34

The motoneuron cell line NSC-34 (tebu-bio, CLU140) was seeded in T75 flasks and cultivated in GM, Dulbecco's modified Eagle's medium (DMEM) containing 4.5 g/L glucose (Gibco) with 10% fetal bovine serum (FBS) (Sigma) and Penicillin-Streptomycin-Glutamine (100X) (Gibco) at 37 °C in an atmosphere of 5% CO_2. Cultures were used between 2–5 passages. NSC-34 cells were only differentiated on a surface coated with Matrigel (Corning Inc., Corning, NY, USA, 354234) in a differentiation medium (NBN2) (Neurobasalmedium (Gibco, 21103049) containing N2 (Gibco, 17502048), murine IGF-1 (Peprotech), MEM non-essential amino acids (Gibco), retinoic acid (BioGems) and Penicillin-Streptomycin-Glutamine (100X) (Gibco)). Cultures were replenished with fresh medium every two days. When the neurite elongation from most of NSC-34 cells was observed under a phase-contrast microscope, they were incubated for 12–18 h with GM containing 1 µg/mL Mitomycin C (Stemcell Technologies, 73274). The NSC-34 cells were then rinsed twice with GM, cultivated for two more days in differentiation medium, NSC-34 cells were detached with Accutase (Gibco, A1110501) prior to co-cultures with differentiating C_2C_{12} cells.

4.3. 3D Co-culture

C_2C_{12} were seeded on a synthetic polystyrene 3D scaffold (Reprocell, *www.reprocell.com*) coated with Laminin (Gibco, 23017015) or Matrigel (Corning) and differentiation was initiated after 2 days of proliferation. NSC-34 cells were added after the differentiation to myotubes in a 3 to 1 ratio. We tested different media for the co-culture to find the optimal environment for both cell types and finally used a modification of the co-culture medium from [50]. In addition, we added Penicillin-Streptomycin-Glutamine (100X) (Gibco) and Agrin (R&D Systems, Inc. Minneapolis, MN, USA, 550-AG). Cultures were replenished with fresh medium every two days.

Seubsequently, we seeded C_2C_{12} in a biological scaffold, a hydrogel based on Collagen type I (Merck Millipore, Darmstadt, Germany, 08115) and Matrigel (Corning) in a 70/30 ratio. C_2C_{12} were proliferated in GM until 70% confluency was reached and differentiated in DM for one or two days. NSC-34 (two days after Mitomycin C treatment) were then seeded on top of the hydrogel in a 1:9 ratio. Medium was then changed to co-culture medium. Cells were grown on hydrogel for several days and analyzed at different time points (4D co-culture).

4.4. Immunocytochemistry

Cultured cells were fixed with ice-cold Roti®Histofix (4% formaldehyde) (Carl Roth GmbH + Co. KG, Karlsruhe, Germany, P087.1) at different time points, and investigated by immunohistochemistry, using different muscle and nerve specific differentiating markers. Prior to staining, the cells were permeabilized and blocked with a blocking buffer containing 0.3% Triton® X-100 (Sigma, 23,472-9), 2% normal goat serum (Invitrogen, 50-197Z) and 2% BSA in 1x TBS (pH 7,4) for 1 h to inhibit nonspecific protein interaction. The samples were then stained using monoclonal antibodies of desmin (1:50; Novocastra Laboratories, Newcastle, UK, NCL-L-DES-DERII), skeletal Myosin (fast) (1:1000; Sigma, M4276) and Neurofilament (1:200; EMD Millipore Corp., Temecula, CA, USA, MAB5266) overnight at 4°C to visualize the junction of developing skeletal muscle fibers with the axons of the motoneurons. The next day, the samples were rinsed in TBS thrice for 2–3 min each to remove any unbound primary antibodies. Subsequently, the slides were incubated in either Alexa 488-conjugated goat anti-mouse IgG (Invitrogen, B13422), Alexa 555-conjugated goat anti-rabbit IgG

 doi:10.20944/preprints202603.0617.v1

(Invitrogen, B35451) or Alexa 635-conjugated goat anti-rabbit IgG (Invitrogen, A31575) at 1:1000 dilution at room temperature for 1 h in dark. In case of multiple first antibodies, there was an additional blocking step with the Mouse Ig Blocking Reagent M.O.M. (Vector Laboratories, Burlingame, CA, USA, MKB-2213) for 2 hours in between. At last, the samples were stained with either Alpha-Bungarotoxin Conjugates Alexa Flour® 488 (1:1000: Invitrogen, B13422) or Alpha-Bungarotoxin Conjugates Alexa Flour® 555 (1:1000; Invitrogen, B35451) for 2 hours in dark. The rinsing step was performed as before and samples were stained for nuclei using the mounting medium with DAPI (Vector Laboratories, H-1400) and covered with cover slips. Digitized z-stacks images were then acquired at high-resolution by using the Leica TCS SP8 confocal microscope, and further processed with the Leica Application Suite X (LAS X) software. Samples incubated with only secondary antibodies were used as controls. All the antibodies were diluted in 2% BSA in TBS prior to use.

4.5. Image analysis

For 3D and distance analysis, we used the LAX Software and 3D Visualization Software (Leica microsystems). The 3D images and videos were captured in the 3D software to better define the viewing angle for better spatial perception of the NMJ. Z-stack images were first processed and set to maximum intensity projection and after further processing the resulting binary image was used as the input for measuring the distance between the axon terminal and the Acetylcholine receptor region. The measured area is the region where the intensity of Population 1 (Axon) decreases and the intensity of Population 2 (AChR) increases which gave us information about the distance between these two opposite microregions in co-cultures.

4.6. Western blot analysis

Total cell extracts were obtained by using the RIPA buffer as Lysis Buffer containing (1% Triton X-100, 150mM NaCl, 50mM TRIS-HCL pH 7,4, 1% (w/v) NP-40, 0,1% (w/v) SDS, 1% (w/v) Na-Deoxycholate plus protease inhibitors (cOmplete Tablet EASYpack, Roche, LOT 41353800)) 10 µl/mg tissue ratio.

Cell sample extracts were mechanically dissolved in the Lysis Bubber by using a tight glass Dounce homogenizer (20 pastel) on ice.

After 20min incubation in the Lysis Buffer, samples were centrifuged with 14.000g for 20min at 4°C. The supernatant fraction was carefully collected and stored at -80°C until used.

Total protein concentration was estimated by using BCA Protein Assay Kit [51] and measured with NanoDrop One (Thermo Fisher Scientific, Waltham, MA, USA) and adjusted to the same protein concentration (1mg/ml) with Laemmli sample buffer (0,5M TRIS, 50% (v/v) Glycerol, 4% (w/v) SDS and 0,02% (w/v) Bromphenolblue) in the presence of reducing agents (700mM DDT, 10% ß-Mercaptoethanol). Reducing condition included an additional heating step to 95°C for 10 min.

Same amount of protein samples was loaded to a 10% Bis-Tris-gel and SDS-PAGE was performed. The gel was blotted on a PVDF-membrane (0,45 µm) at 100V for 60min at 15 °C. Preincubation with a blocking solution containing 2% (w/v) slim milk powder (SERVA, 425590.01, LOT 200120). Incubation was done at room temperature for 60min. Specific mouse anti-desmin IgG1 antibodies were used from (MONOSAN Xtra, Clone DE-R-11, Cat. No. MONX10657), 1:250, 60min, RT to detect the desmin proteins. Fluorescence conjugated secondary antibodies Alexa Fluo-555 goat anti-mouse (Invitrogen, A21147, 1:500, 60 min at RT) were used in block solution to detect the primary antibodies.

The membranes were scanned with the Azure400 Fluorescent Imager (Azure Biosystems, Dublin, CA, USA) and analyzed with ImageJ Software [52]. The image has been subjected first to channel splitting, followed by a background subtraction with a rolling ball radius of 50 pixels and selected sliding paraboloid. The ROIs with cleared signal was set by the Threshold function with dark background, applied and after the function Analyze Particles, the ROIs has been added to the ROI Manager. The selected ROIs have been analyzed on the raw image using the Measure function,

 doi:10.20944/preprints202603.0617.v1

focusing on the area of signal, mean gray scale value, max and min gray scale value and integrated density as the total fluorescence signal within the selected ROIs.

4.7. qPCR analysis

Total RNA from the cells in hydrogel was extracted using Trizol® (Invitrogen; Thermo Fisher Scientific, Inc., 15596026) and the PureLink RNA Mini Kit (Invitrogen, 12183025) according to the manufacturer's protocol. All steps after RNA extraction leading to the RNA sequencing were handled by the Charité Berlin Institute of Health (BIH) Core Facility Genomics.

4.8. RNA extraction and quantitative PCR (qPCR)

Total RNA was obtained from cell cultures (2 different time curve samples for each cell line and for co-culture were used) using TRIzol® (Thermo Fisher Scientific, USA) extraction method, according to the manufacturer's instructions. 1 mg of RNA was converted to cDNA by using random hexamers and SuperScript® VILO™ (Thermo Fisher Scientific, USA) following the manufacturer's instructions. Specific primers for SNAP25, Jph1 and RyR1 were designed using Primer3 software (https://primer3.org/). Thermodynamic specificity was determined using BLAST sequence alignment (NCBI) and vector NTI® software (https://vector-nti.software.informer.com/).

Primer sequences were as follows:

m_SNAP25_fw	CGCAATGAGCTGGAGGAGAT
m_SNAP25_rv	TCGCCTTGCTCATCCAACAT
m_Jph1_fw	GCAAGCAATGATACCTGCCC
m_Jph1_rv	AAGGCTATGCTTACCTGTCCTAA
m_RyR1_fw	GGCAGATGAGAAGGCAGAAG
m_RyR1_rv	TCCACCAGAGTTGTCTGTGC

qPCR was performed in a CFX Connect® Real time System (Bio-Rad, USA) using SYBR Green chemistry. All samples were run in triplicate and simultaneously with RNA-negative controls. Cyclophilin A (PPIA), Hypoxanthine Phosphoribosyl transferase 1 (HPRT1) and TATA-Box Binding Protein (TBP) were tested as candidate reference genes, being the latter the most stable to normalize Ct values. Primers sequences were published elsewhere [53]. Normalization was performed by ΔCt method.

4.9. Statistical analysis

The Linear Mixed Effects Model was used for statistical analysis. Data analysis was performed using GraphPad Prism software. Results were considered statistically significant at a predefined level of $p \leq 0.05$ confidence. All graphs were created with GraphPad Prism5 software.

5. Conclusions

Given the increasing need for *in vitro* experimental models and tissue engineering methodologies, especially for physiological/pathophysiological and pharmacological studies, we have established a robust and powerful tool (3D NErve and MUscle CO-culture, NEMUCO) to study structural and molecular dynamic evolution during time (the 4th dimension, 4D co-culture). This model enables deeper insights into major characteristics of NMJ synaptogenesis, from microarchitecture to underlying mechanisms reflected by defined molecular expression profiles, replicated under well-defined 3D *in vitro* culture conditions. *In vitro* modeling of the NMJ represents a useful tool for studying cellular/subcellular and molecular events leading to subcellular organization of key molecular players in pre- and postsynaptic NMJ microdomains, applicable in various experimental settings from fundamental to clinical research laboratories.

In addition to cell models grown on specialized biological chips [25,49], standardized 3D neuron-muscle co-cultures from well-characterized single cell lines reported here provide a reliable research platform for studying temporal and spatial hierarchical assembly of molecular players

 doi:10.20944/preprints202603.0617.v1

regulating synaptogenesis, NMJ stability, adaptation, and plasticity. This model can be also used for testing therapeutic pharmacological approaches or treatments capable of restoring impaired NMJ transmission in different neurodegenerative clinical settings, including autoimmune neuromuscular diseases like myasthenia gravis, and in conditions of altered muscle activity in microgravity and/or during aging.

Author Contributions: Conceptualization MS; writing—original draft preparation, MS, DB, PV, PL, IV; validation, KB, GZ, GT, SF, SA, MG; supervision and editing, MS; project administration, MS. All authors have read and agreed to the published version of the manuscript.

Funding: Bundesministerium für Forschung, Technologie und Raumfahrt (BMFTR) through the German Space Agency, Deutsches Zentrum für Luft- und Raumfahrt (DLR e.V., Bonn-Oberkassel, Germany): 50WB1826, 50WB2116 and 50WB2416 (to MS). Grant Programma-Contratto ASI, 2018-13-U.0-NEMUCO (to PV and PL).:.

Institutional Review Board Statement: Not applicable.

Informed Consent Statement: Not applicable.

Data Availability Statement: No new data were created or analyzed in this study. Data sharing is not applicable to this article.

Acknowledgments: We acknowledge Reprocell for their technical support with the synthetic 3D scaffold and all the people who are not listed as coauthors which directly or indirectly contributed to this study.

Conflicts of Interest: The authors declare no conflict of interest. The sponsors had no role in the design, execution, interpretation, or writing of the study.

References

1. Salanova, M., Bortoloso, E., Schiffl, G., Gutsmann, M., Belavy, D. L., Felsenberg, D., Furlan, S., Volpe, P., and Blottner, D. (2011) Expression and regulation of Homer in human skeletal muscle during neuromuscular junction adaptation to disuse and exercise. *FASEB J* **25**, 4312–4325
2. Iyer, S. R., Shah, S. B., and Lovering, R. M. (2021) The Neuromuscular Junction: Roles in Aging and Neuromuscular Disease. *Int J Mol Sci* **22**
3. Huijbers, M. G., Marx, A., Plomp, J. J., Le Panse, R., and Phillips, W. D. (2022) Advances in the understanding of disease mechanisms of autoimmune neuromuscular junction disorders. *Lancet Neurol* **21**, 163–175
4. Murgia, M., Rittweger, J., Reggiani, C., Bottinelli, R., Mann, M., Schiaffino, S., and Narici, M. V. (2024) Spaceflight on the ISS changed the skeletal muscle proteome of two astronauts. *NPJ Microgravity* **10**, 60
5. Blottner, D., Moriggi, M., Trautmann, G., Hastermann, M., Capitanio, D., Torretta, E., Block, K., Rittweger, J., Limper, U., Gelfi, C., and Salanova, M. (2023) Space Omics and Tissue Response in Astronaut Skeletal Muscle after Short and Long Duration Missions. *Int J Mol Sci* **24**
6. Bao, Z., Cui, C., Chow, S. K., Qin, L., Wong, R. M. Y., and Cheung, W. H. (2020) AChRs Degeneration at NMJ in Aging-Associated Sarcopenia-A Systematic Review. *Front Aging Neurosci* **12**, 597811
7. Blottner, D., Trautmann, G., Furlan, S., Gambara, G., Block, K., Gutsmann, M., Sun, L. W., Worley, P. F., Gorza, L., Scano, M., Lorenzon, P., Vida, I., Volpe, P., and Salanova, M. (2021) Reciprocal Homer1a and Homer2 Isoform Expression Is a Key Mechanism for Muscle Soleus Atrophy in Spaceflown Mice. *Int J Mol Sci* **23**
8. Moss, K. R., Darvishi, F. B., Badawi, Y., Fish, L. A., Funke, J. R., Pedersen, T. H., Robitaille, R., Arnold, W. D., Burgess, R. W., Meriney, S. D., Nishimune, H., and Saxena, S. (2025) The Neuromuscular Junction: A Shared Vulnerability in Aging and Disease. *J Neurosci* **45**
9. Sanes, J. R., and Lichtman, J. W. (1999) Development of the vertebrate neuromuscular junction. *Annu Rev Neurosci* **22**, 389–442

 doi:10.20944/preprints202603.0617.v1

10. Davis, L. A., Fogarty, M. J., Brown, A., and Sieck, G. C. (2022) Structure and Function of the Mammalian Neuromuscular Junction. *Compr Physiol* **12**, 3731–3766
11. Hyman, S. E. (2005) Neurotransmitters. *Curr Biol* **15**, R154–158
12. Mukund, K., and Subramaniam, S. (2020) Skeletal muscle: A review of molecular structure and function, in health and disease. *Wiley Interdiscip Rev Syst Biol Med* **12**, e1462
13. Mis, K., Grubic, Z., Lorenzon, P., Sciancalepore, M., Mars, T., and Pirkmajer, S. (2017) In Vitro Innervation as an Experimental Model to Study the Expression and Functions of Acetylcholinesterase and Agrin in Human Skeletal Muscle. *Molecules* **22**
14. Andersen, J., Revah, O., Miura, Y., Thom, N., Amin, N. D., Kelley, K. W., Singh, M., Chen, X., Thete, M. V., Walczak, E. M., Vogel, H., Fan, H. C., and Pasca, S. P. (2020) Generation of Functional Human 3D Cortico-Motor Assembloids. *Cell* **183**, 1913–1929 e1926
15. Barbeau, S., Tahraoui-Bories, J., Legay, C., and Martinat, C. (2020) Building neuromuscular junctions in vitro. *Development* **147**
16. Zhang, K., Bai, L., Xu, W., and Shen, C. (2022) Human neuromuscular junction three-dimensional organoid models and the insight in motor disorders. *J Mol Cell Biol* **13**, 767–773
17. Yaffe, D., and Saxel, O. (1977) Serial passaging and differentiation of myogenic cells isolated from dystrophic mouse muscle. *Nature* **270**, 725–727
18. Nango, H., Kosuge, Y., Sato, M., Shibukawa, Y., Aono, Y., Saigusa, T., Ito, Y., and Ishige, K. (2020) Highly Efficient Conversion of Motor Neuron-Like NSC-34 Cells into Functional Motor Neurons by Prostaglandin E(2). *Cells* **9**
19. Knight, E., Murray, B., Carnachan, R., and Przyborski, S. (2011) Alvetex(R): polystyrene scaffold technology for routine three dimensional cell culture. *Methods Mol Biol* **695**, 323–340
20. Zhang, Y., Xu, Y., and Gao, J. (2023) The engineering and application of extracellular matrix hydrogels: a review. *Biomater Sci* **11**, 3784–3799
21. Lin, S., Landmann, L., Ruegg, M. A., and Brenner, H. R. (2008) The role of nerve- versus muscle-derived factors in mammalian neuromuscular junction formation. *J Neurosci* **28**, 3333–3340
22. DeChiara, T. M., Bowen, D. C., Valenzuela, D. M., Simmons, M. V., Poueymirou, W. T., Thomas, S., Kinetz, E., Compton, D. L., Rojas, E., Park, J. S., Smith, C., DiStefano, P. S., Glass, D. J., Burden, S. J., and Yancopoulos, G. D. (1996) The receptor tyrosine kinase MuSK is required for neuromuscular junction formation in vivo. *Cell* **85**, 501–512
23. Yang, X., Arber, S., William, C., Li, L., Tanabe, Y., Jessell, T. M., Birchmeier, C., and Burden, S. J. (2001) Patterning of muscle acetylcholine receptor gene expression in the absence of motor innervation. *Neuron* **30**, 399–410
24. Kim, H., Kim, G. S., Hyun, S. H., and Kim, E. (2023) Advancements in 2D and 3D In Vitro Models for Studying Neuromuscular Diseases. *Int J Mol Sci* **24**
25. Leng, Y., Li, X., Zheng, F., Liu, H., Wang, C., Wang, X., Liao, Y., Liu, J., Meng, K., Yu, J., Zhang, J., Wang, B., Tan, Y., Liu, M., Jia, X., Li, D., Li, Y., Gu, Z., and Fan, Y. (2023) Advances in In Vitro Models of Neuromuscular Junction: Focusing on Organ-on-a-Chip, Organoids, and Biohybrid Robotics. *Adv Mater* **35**, e2211059
26. Nebol, A., and Gouti, M. (2024) A new era in neuromuscular junction research: current advances in self-organized and assembled in vitro models. *Curr Opin Genet Dev* **87**, 102229
27. Luttrell, S. M., Smith, A. S. T., and Mack, D. L. (2021) Creating stem cell-derived neuromuscular junctions in vitro. *Muscle Nerve* **64**, 388–403
28. Qaisar, R. (2023) Targeting neuromuscular junction to treat neuromuscular disorders. *Life Sci* **333**, 122186
29. Lotti, F., and Przedborski, S. (2022) Motoneuron Diseases. *Adv Neurobiol* **28**, 323–352
30. Redden, J. T., Kothe, S., Cohen, D. J., Schwartz, Z., and McClure, M. J. (2025) Trophic Factors in Muscle-Nerve Cross-Talk Signaling Augment Muscle Fiber and Motor Endplate Development. *J Cell Physiol* **240**, e70013
31. Justus, C. R., Marie, M. A., Sanderlin, E. J., and Yang, L. V. (2023) Transwell In Vitro Cell Migration and Invasion Assays. *Methods Mol Biol* **2644**, 349–359

 doi:10.20944/preprints202603.0617.v1

32. Liu, Y., Padgett, D., Takahashi, M., Li, H., Sayeed, A., Teichert, R. W., Olivera, B. M., McArdle, J. J., Green, W. N., and Lin, W. (2008) Essential roles of the acetylcholine receptor gamma-subunit in neuromuscular synaptic patterning. *Development* **135**, 1957–1967
33. Schubert, M., Pelz, A., Trautmann, G., Block, K., Furlan, S., Gutsmann, M., Kohler, S., Volpe, P., Blottner, D., Meisel, A., and Salanova, M. (2022) Opposite Regulation of Homer Signal at the NMJ Postsynaptic Micro Domain between Slow- and Fast-Twitch Muscles in an Experimentally Induced Autoimmune Myasthenia Gravis (EAMG) Mouse Model. *Int J Mol Sci* **23**
34. Melnik, D., Kruger, M., Schulz, H., Kopp, S., Wehland, M., Bauer, J., Baselet, B., Vermeesen, R., Baatout, S., Corydon, T. J., Infanger, M., and Grimm, D. (2021) The CellBox-2 Mission to the International Space Station: Thyroid Cancer Cells in Space. *Int J Mol Sci* **22**
35. Baranski, S., and Marciniak, M. (1990) Morphometric ultrastructural analysis of muscle fibers and neuromuscular junction in rats kept under conditions of weightlessness for 21 days. *Mater Med Pol* **22**, 258–262
36. Deschenes, M. R., Wilson, M. H., and Kraemer, W. J. (2005) Neuromuscular adaptations to spaceflight are specific to postural muscles. *Muscle Nerve* **31**, 468–474
37. Pozdniakov, O. M., Babakova, L. L., Demorzhi, M. S., and Il'ina-Kakueva, E. I. (1990) [Changes in the ultrastructure of striated muscles and neuromuscular synapses of rats under the effects of a 13-day space flight]. *Kosm Biol Aviakosm Med* **24**, 38–42
38. Nishimune, H., Stanford, J. A., and Mori, Y. (2014) Role of exercise in maintaining the integrity of the neuromuscular junction. *Muscle Nerve* **49**, 315–324
39. Edgerton, V. R., and Roy, R. R. (1994) Neuromuscular adaptation to actual and simulated weightlessness. *Adv Space Biol Med* **4**, 33–67
40. Roy, R. R., Baldwin, K. M., and Edgerton, V. R. (1996) Response of the neuromuscular unit to spaceflight: what has been learned from the rat model. *Exerc Sport Sci Rev* **24**, 399–425
41. Salanova, M., Gambara, G., Moriggi, M., Vasso, M., Ungethuem, U., Belavy, D. L., Felsenberg, D., Cerretelli, P., Gelfi, C., and Blottner, D. (2015) Vibration mechanosignals superimposed to resistive exercise result in baseline skeletal muscle transcriptome profiles following chronic disuse in bed rest. *Sci Rep* **5**, 17027
42. Antonutto, G., Capelli, C., Girardis, M., Zamparo, P., and di Prampero, P. E. (1999) Effects of microgravity on maximal power of lower limbs during very short efforts in humans. *J Appl Physiol (1985)* **86**, 85–92
43. Edgerton, V. R., Zhou, M. Y., Ohira, Y., Klitgaard, H., Jiang, B., Bell, G., Harris, B., Saltin, B., Gollnick, P. D., Roy, R. R., and et al. (1995) Human fiber size and enzymatic properties after 5 and 11 days of spaceflight. *J Appl Physiol (1985)* **78**, 1733–1739
44. Baranski, S., Baranska, W., Marciniak, M., and Ilyina-Kakueva, E. I. (1979) Ultrasonic investigations of the soleus muscle after space flight on the Biosputnik 936. *Aviat Space Environ Med* **50**, 930–934
45. D'Amelio, F., and Daunton, N. G. (1992) Effects of spaceflight in the adductor longus muscle of rats flown in the Soviet Biosatellite COSMOS 2044. A study employing neural cell adhesion molecule (N-CAM) immunocytochemistry and conventional morphological techniques (light and electron microscopy). *J Neuropathol Exp Neurol* **51**, 415–431
46. Riley, D. A., Ilyina-Kakueva, E. I., Ellis, S., Bain, J. L., Slocum, G. R., and Sedlak, F. R. (1990) Skeletal muscle fiber, nerve, and blood vessel breakdown in space-flown rats. *FASEB J* **4**, 84–91
47. Deschenes, M. R., Britt, A. A., Gomes, R. R., Booth, F. W., and Gordon, S. E. (2001) Recovery of neuromuscular junction morphology following 16 days of spaceflight. *Synapse* **42**, 177–184
48. Wilson, M. H., and Deschenes, M. R. (2005) The neuromuscular junction: anatomical features and adaptations to various forms of increased, or decreased neuromuscular activity. *Int J Neurosci* **115**, 803–828
49. Alavi-Moghadam, S., Kokabi-Hamidpour, S., Rezaei-Tavirani, M., Larijani, B., Arjmand, R., Rahim, F., Rezazadeh-Mafi, A., Adibi, H., and Arjmand, B. (2024) Neuromuscular Junction-on-a-Chip for Amyotrophic Lateral Sclerosis Modeling. *Methods Mol Biol* **2736**, 139–150
50. Guo, X., Das, M., Rumsey, J., Gonzalez, M., Stancescu, M., and Hickman, J. (2010) Neuromuscular junction formation between human stem-cell-derived motoneurons and rat skeletal muscle in a defined system. *Tissue Eng Part C Methods* **16**, 1347–1355

 doi:10.20944/preprints202603.0617.v1

51. Smith, P. K., Krohn, R. I., Hermanson, G. T., Mallia, A. K., Gartner, F. H., Provenzano, M. D., Fujimoto, E. K., Goeke, N. M., Olson, B. J., and Klenk, D. C. (1985) Measurement of protein using bicinchoninic acid. *Anal Biochem* **150**, 76–85
52. Schneider, C. A., Rasband, W. S., and Eliceiri, K. W. (2012) NIH Image to ImageJ: 25 years of image analysis. *Nat Methods* **9**, 671–675
53. Gambara, G., Salanova, M., Ciciliot, S., Furlan, S., Gutsmann, M., Schiffl, G., Ungethuem, U., Volpe, P., Gunga, H. C., and Blottner, D. (2017) Microgravity-Induced Transcriptome Adaptation in Mouse Paraspinal longissimus dorsi Muscle Highlights Insulin Resistance-Linked Genes. *Front Physiol* **8**, 279